Two-Dimensional Nanomaterials in Organic Solar Cells

Subjects: Materials Science, Coatings & Films
Contributor: Shenghua LIU

The thin-film organic solar cells (OSCs) are currently one of the most promising photovoltaic technologies to effectively harvest the solar energy due to their attractive features of mechanical flexibility, light weight, low-cost manufacturing, and solution-processed large-scale fabrication, etc. However, the relative insufficient light absorption, short exciton diffusion distance, and low carrier mobility of the OSCs determine the power conversion efficiency (PCE) of the devices are relatively lower than their inorganic photovoltaic counterparts. To conquer the challenges, the two-dimensional (2D) nanomaterials, which have excellent photoelectric properties, tunable energy band structure, and solvent compatibility etc., exhibit the great potential to enhance the performance of the OSCs.

Keywords: organic solar cells ; 2D materials ; additives ; active layer ; charge transporting layer

1. Introduction

Globe environment pollution and energy crisis have become the major issues accompanied with the economic growth owing to the excessive consumption of fossil resources. Searching for alternative renewable energy is one of the most significant technologies to solve the urgent problems [1][2]. Solar energy has become an ideal energy resource due to its inexhaustible, widespread, and environmentally friendly characteristics, which can be effectively exploited and converted into electricity [3][4][5][6]. Organic solar cells (OSCs) as one of the third-generation photovoltaics have achieved rapid development currently, which exhibit great advantages for their low cost, light weight, simple manufacture, and large-area fabrication [7][8][9]. In recent years, the performance of the OSCs has been dramatically improved with the emergence of the non-fullerene acceptor and the relevant donor materials [7][10][11][12][13][14][15], which leads to the tremendous breakthroughs in power conversion efficiencies (PCE) of the OSCs. According to the theoretical calculations, it is reported the highest efficiency of the single-junction non-fullerene acceptor-based OSCs (NFA-OSCs) is expected to exceed 20% [16][17][18][19][20][21]. However, the NFA-OSCs are still confronted with several challenges compared with other high-efficient photovoltaics. Particularly, the relatively low device efficiency and long-term instability of the OSCs limit their industrial production and commercialization [22][23][24]. The serious electron-hole recombination, low carrier mobility of the active layers, and insufficient sunlight absorption are taking the main responsibility for the limited PCE of the OSCs. Besides, it is well acknowledged that the most commonly used hole transport layer (HTL) material, Poly(3,4-ethylenedioxythiophene):poly(styrenesulfonate) (PEDOT:PSS) exhibits hygroscopicity characteristic, which can easily corrode the indium tin oxide (ITO) electrode material, decreasing the efficiency and stability of the devices [25][26][27][28][29].

Lots of strategies have been applied to improve the efficiency and stability of the OSCs [4][11][12][18]. For example, the introduction of metal nanostructures into the OSCs can increase the light absorption capacity of the active layer with a plasma enhancement effect [30][31][32], increasing the PCE of photovoltaic devices. Owing to the quantum size effect, the addition of quantum dots into the active layer of the OSCs can harvest more sunlight from the wider band of the solar spectrum for enhancing the efficiency of the devices [33][34][35][36]. Nanowires with conductive properties can replace ITO as electrode materials of the OSCs with superior stability and competitive photovoltaic performances [37][38][39][40][41].

Among the variety of the nanomaterials applied in the OSCs, 2D layered materials can be considered as promising candidates for the application in different positions of the OSCs due to their excellent optoelectronic characteristics, tunable energy band structure, and relatively stable physical and chemical properties [42][43][44][45][46][47][48]. Most of the 2D nanomaterials have a typical layered structures with solution-processability [6][25][26][38][44][45]. In **Table 1**, we list a few typical 2D materials and their key physical parameters. The 2D materials, such as WSe_2, BP, etc. with tunable bandgaps exhibit carrier mobilities several orders of magnitude higher than those of the organic semiconductors in OSCs.

Table 1. The physical parameters of a few novel 2D materials applied in OSCs.

Materials	Bandgap (eV)	Carrier Mobility ($cm^2 V^{-1} s^{-1}$)	Ref.
WSe_2	1.2–1.7	500	[49]
$MoSe_2$	1.5	50	[50]

Materials	Bandgap (eV)	Carrier Mobility ($cm^2 V^{-1} s^{-1}$)	Ref.
Bi_2O_2S	1.27	16,000–26,000	[51]
α-In_2Se_3	1.5–2.8	2.5	[52]
BP	0.3–2.0	1000	[53]
$Ti_3C_2T_x$	0–3.4	0.70	[54]
Graphene	0	1000	[55]
MoS_2	1.2–1.8	10–200	[56]

The incorporation of suitable 2D materials into the OSCs, not only can enhance the light absorption and scattering in the devices, but also improve the charge transport and suppress the carrier recombination, leading to an enhancement of PCE with the increased fill factor (FF) and short-circuit current density (Jsc) of the OSCs. Besides, appropriate 2D materials can replace the unstable PEDOT:PSS layer or evaporated electrodes for improving the stability and simplifying the fabrication process of the OSCs.

2. The Application of 2D Materials in the Active Layer

To achieve high-performance OSCs, 2D materials involved in the active layer of the photovoltaic devices as the third components have aroused widespread concerns. Graphene has attracted tremendous attention since being synthesized in 2004 [57], which possess excellent carrier mobility. And its derivative graphene oxide (GO) by solution-processable exfoliation of graphene has also been extensively studied in the field of organic optoelectronic devices due to the high carrier mobility, great conductivity, and solution dispersibility at the presence of oxygen functional groups [58][59][60][61][62]. In 2015, Stylianakis et al. synthesized the graphene-based porphyrin molecule (GO-TPP) as an additive in the active layer of OSCs [63]. Simply by covalent interaction between the GO and 5-(4-aminophenyl)-10,15,20-triphenyl) porphyrin (TPP-NH_2) as shown in **Figure 1**a, the TPP-NH_2 porphyrin presents π aromatic framework with excellent stability and light-harvesting capacity. As presented in **Figure 1**b, the OSCs based on PCDTBT:$PC_{71}BM$ and PTB7:$PC_{71}BM$ were fabricated, respectively, which exhibited the device structure of ITO/PEDOT:PSS/Active layer + GO-TTP/TiO_x/Ca/Al. The incorporation of GO-TPP enabled to optimize the band structure of the device with cascaded energy levels between the donor and acceptor as shown in **Figure 1**c. Moreover, it provided continuous penetration paths between the donor and acceptor interfaces, which led to the suppression of exciton recombination and the promotion of charge transport. As shown in **Figure 1**d,e. The best PCEs of 7.13% and 8.81% in the PCDTBT:$PC_{71}BM$ and PTB7:$PC_{71}BM$-based OSCs were achieved, respectively by adding the optimum concentration of 0.3% GO-TPP.

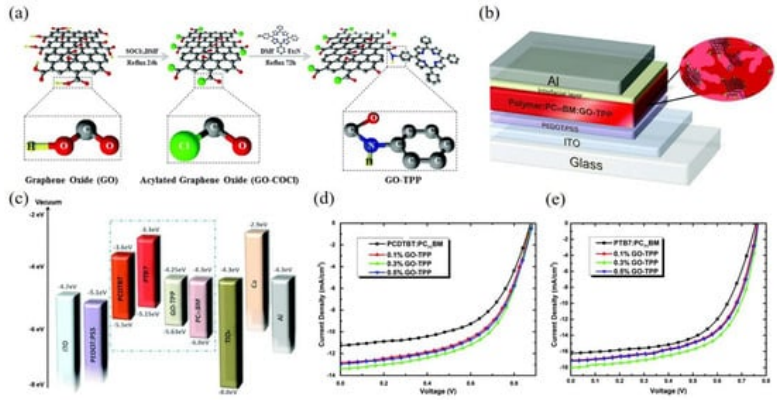

Figure 1. Schematic representation of (**a**) the chemical synthesis of GO-TPP and (**b**) the photovoltaic device; (**c**) Energy level diagram of the photovoltaic device; The J-V curves of the OSCs based on (**d**) PCDTBT:$PC_{71}BM$ and (**e**) PTB7:$PC_{71}BM$ with different concentrations of GO-TPP. Reprinted with permission from [63]. Copyright 2015 The Royal Society of Chemistry.

Among the variety of 2D nanomaterials, besides graphene and its derivatives, transition metal dichalcogenides (TMDs) are the most widely studied materials, which are formed by the transition metal atom such as W, Mo, Pd, Pt et al. sandwiched among the chalcogenide atoms such as Se, S, Te. TMDs like WSe_2 that have been studied in the early, exhibits high mobility around 500 $cm^2 V^{-1} s^{-1}$ and 10^4 on/off ratios at 60 k. MoS_2 is also a popular TMD material with high mobility of 200 $cm^2 V^{-1} s^{-1}$ at room temperature. The bandgap of 2D WS_2 is more than 2 eV, while the 2D MoS_2 is approximately 1.2–1.9 eV. The TMDs with different thicknesses related to the nanoscale domain sizes of the active layer have distinctly different effects on the performance of the OSCs.

In 2017, Kymakis et al. incorporated WSe_2 flakes into the active layer of PTB7:$PC_{71}BM$-based OSCs [64]. As shown in **Figure 2**a. They exploited the sedimentation-based separation to sort the WSe_2 flakes by ultracentrifugation with different centrifugal speeds, which obtained different sizes of WSe_2 with ~70, ~240, and ~720 nm^2, respectively (see **Figure 2**b–d). The structure of the device based on PTB7:$PC_{71}BM$:WSe_2 was displayed in **Figure 2**e. The bandgap of WSe_2 could be tuned with the thickness variation from 0.8 eV in the bulk to 1.3 eV in the single layer, which provides matchable energy levels to improve the carrier mobility, exciton dissociation, and charge extraction (seen in **Figure 2**f). It is demonstrated that the incorporation of WSe_2 flakes with a similar size to the domain of the active layer led to the best PCE s for the OSCs due to the optimized percolation pathways for charge transport. Therefore, the champion devices based on PTB7:$PC_{71}BM$ with the incorporation of ~240 nm^2 WSe_2 achieved the PCE of 9.45%, enhancing by 16.67% compared with the control devices, as shown in **Figure 2**g. This research quantitatively illustrated the relationship between the 2D nanomaterial and domain sizes of the active layer, indicating the effective strategy to control the area and thickness of the 2D materials for improving the photovoltaic performance of the OSCs and other photovoltaics.

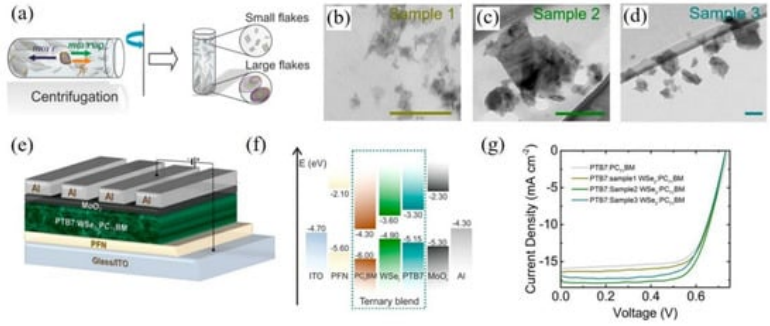

Figure 2. Schematic representation of (**a**) the fabrication of WSe_2 flakes by ultracentrifugation depended on SBS method and the separation of different sizes of WSe_2 flakes; TEM images of WSe_2 flakes with different area values of (**b**) ~70, (**c**) ~240 and (**d**) ~720nm^2, respectively; (**e**) The device structure of ternary OSCs with incorporation of WSe_2 flakes in the active layer; (**f**) Schematic energy levels and (**g**) J-V curves of the OSCs based on PTB7:$PC_{71}BM$. Reprinted with permission form [64]. Copyright 2017 American Chemical Society.

To further enrich the application of 2D TMDs materials in the OSCs, it is of necessity to exploit new methods for the functionalization of TMDs materials. In 2019, Wei et al. adopted the hydrogen plasma treatment to modify the properties of $MoSe_2$ as shown in **Figure 3**a [65]. Hydrogenated $MoSe_2$ nanosheets will form the H-Se-Mo bonds, which can lead to the electron transfer from the hydrogen atoms to the selenium atoms, enhancing the repulsive forces among selenium atoms and increasing the quantities of the produced photoelectrons. Hydrogenated $MoSe_2$ was subsequently applied in the OSCs based on PTB7-Th:$PC_{71}BM$ in the active layer as displayed in **Figure 3**b. The incorporation of hydrogenated $MoSe_2$ in the ternary blend optimized the morphology of the active layer and served as additional conducting bridges for the charge transfer, improving the carrier mobility in the devices (seen in **Figure 3**c). As shown in **Figure 3**d,e, the champion devices based on PTB7-Th:$PC_{71}BM$ and PBDTTBOIT-4F reached 10.44% and 8.13%, respectively by incorporating the hydrogen plasma-treated $MoSe_2$ nanosheets in the active layer. Moreover, hydrogenated TMDs show great stability owing to the shorter bonding distance between the chalcogen atoms and hydrogen atoms than those between the chalcogen atoms and other atoms from density functional theory calculations. Thus, after thermal treatment at 100 °C for 1 h, the devices with the hydrogenated $MoSe_2$ maintained 70% of the original PCE compared with the reference devices with 60%, as exhibited in **Figure 3**f.

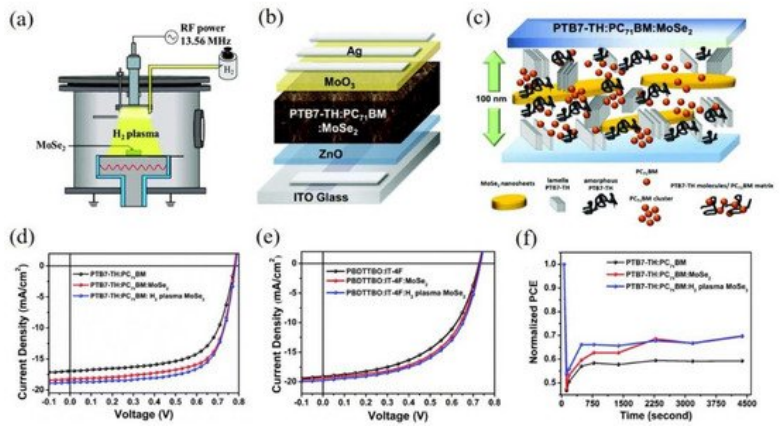

Figure 3. (**a**) Schematic representation of the H_2 plasma treatment; (**b**) The device structure of inverted OSCs based on PTB7-Th:$PC_{71}BM$ with $MoSe_2$; (**c**) Schematic diagram of the interplay of $MoSe_2$ with PTB7-TH and $PC_{71}BM$; J-V characteristics of (**d**) PTB7-Th:$PC_{71}BM$ and (**e**) PBDTTBO:IT-4F devices without $MoSe_2$ and introducing $MoSe_2$ with and without hydrogen plasma treatment; (**f**) Stability of PCE values of devices based on PTB7-TH:$PC_{71}BM$ without $MoSe_2$ and

adding $MoSe_2$ with and without hydrogen plasma treatment at 100 °C. Reprinted with permission form [65]. Copyright 2019 The Royal Society of Chemistry.

2D Black phosphorus (BP) is another novel layered semiconductor with an allotrope of phosphorus, which has extraordinarily high charge mobilities of about ~1000 $cm^2\ V^{-1}\ s^{-1}$ [45][55][56]. The bandgap of BP is adjustable from 0.3 to 1.8, and 2.1 eV, corresponding to the bulk, bilayers, and monolayer, respectively, which enables BP to match well with the bandgap of the donor and acceptor in the OSCs.

In 2019, Chen et al. studied the application of the embedded BP nanoflakes in the active layer of OSCs [66]. They used the liquid-phase exfoliation method to fabricate BP nanoflakes with the size of 46 nm and re-dispersed them in chlorobenzene. The incorporation of BP nanoflakes can form the π-π stacking ordering and optimize the phase purity of the active layer, contributing to the improved charge mobilities and suppressed charge recombination. As a result, the PCE of 12.2% can be obtained for the OSCs based on PTB7-Th:IEICO-4F with the Jsc of 23.94 mA cm^{-2}, Voc of 0.72 V, and FF of 0.73. Besides, the thermal stability of the device with BP nanoflakes was investigated by thermal treatment at 150 °C, which remains 73% of the original PCE compared with the reference device of 60%.

However, the traditional exfoliation method for the fabrication of BP may limit the application due to the poor dispersibility of BP clusters in organic solvents. Liu et al. exhibited a one-step solvothermal method to produce BP from the cheap and available white phosphorus and also incorporated them into the active layer of the OSCs [67]. Due to the noncovalent interactions between PTB7-Th and BP, the uniform and continuous active layer can be observed in the AFM image as shown in **Figure 4**a, additionally, the 2D GIWAXS patterns (see **Figure 4**b,c) displayed similar diffraction patterns in the active layer with or w/o BP incorporation, which illustrated the BP hardly affected the crystallization of donor and acceptor and the phase separation of the active layer. As indicated in **Figure 4**d, the PCE of 10.5% was realized in the device based on PTB7-Th:$PC_{71}BM$ incorporating with 10 wt% BP in the active layer, resulting from the improvement of the carrier mobility and charge collection.

Carrier mobility is one of the key factors to determine the device performance A few 2D materials like bismuth oxychalcogenides (Bi_2O_2X) have a large surface area with excellent carrier mobility and high electron affinity, which can be applied in the photovoltaics [68][69]. Besides, the Bi_2O_2X, such as Bi_2O_2S, Bi_2O_2Se and Bi_2O_2Te have suitable bandgaps about 1.27 eV, 0.8 eV and 0.11 eV, respectively. In 2019, Huang et al. reported the 2D Bi_2O_2S as a potential candidate for the performance improvement of the OSCs [70]. The Bi_2O_2S nanomaterial synthesized by the hydrothermal method was incorporated into the PTB7:$PC_{71}BM$-based binary OSCs. The results showed that the Bi_2O_2S nanomaterial with a suitable energy band structure is matchable with the donor and acceptor materials, which can promote the exciton dissociation and charge transfer in the active layer. As a result, the PCE of the ternary OSCs by incorporating the 1 wt% Bi_2O_2S nanomaterial was improved from 8.79% to 10.71% compared with the binary OSCs.

Another 2D Bi_2O_2Se nanoflakes have high carrier mobility about 450 $cm^2\ V^{-1}\ s^{-1}$ at room temperature with a tunable bandgap about 1.9 eV in monolayer and 0.8eV in bulk [71][72][73][74][75]. In 2020, Huang et al. fabricated the 2D Bi_2O_2Se nanoflakes by liquid-phase exfoliation with lithium intercalation and incorporate them into the active layer of the OSCs as an additive [76]. It was suggested that the 2D Bi_2O_2Se nanoflakes not only promoted the crystallization of the active layer and optimized the interpenetrating networks, but also increased the contact area between the donor and acceptor and provide efficient charge transfer pathways, improving the exciton separation and charge transfer in the active layer. The optimized ternary OSCs with the addition of 2 wt% Bi_2O_2Se nanoflakes presented the PCE of 16.28% based on PM6:Y6 blend active layer compared with the 14.59% of the binary device. Meanwhile, the devices incorporated with 2D Bi_2O_2Se nanoflakes exhibited remarkable stability in the air for 30 days without any encapsulation. The OSCs within 2 wt% Bi_2O_2Se nanoflakes remained 91% of the original PCE, while the control devices only remained 77%, which was mainly attributed to the better morphology stability and higher crystallization of the active layer with Bi_2O_2Se incorporation.

Mxene is another novel 2D material with outstanding optoelectronic performance, which consists of transition metal carbides, nitrides, or carbonitrides with a thickness of several atomic layers [77][78]. They have extra high conductivity due to the hydroxyl or terminal oxygen on the surface of MXene. Recently, Zhao et al. incorporated the solution-processed MXene material, titanium carbide ($Ti_3C_2T_x$) nanosheets into the active layer of OSCs as shown in **Figure 4**e, obtaining an improvement in the device performance [79]. The additive almost not affected the interpenetrating network morphology, and further provided an alternative way for the charge transport within the active layer. As revealed in **Figure 4**f, the $Ti_3C_2T_x$ nanosheets boosted the light-harvesting of the active layer, leading to the significant enhancement in J_{sc} from 24.72 mA cm^{-2} to 27.02 mA cm^{-2} based on PM6:Y6-based OSCs. It was worth noting that the addition of $Ti_3C_2T_x$ nanosheets improves the exciton dissociation, optimizes the charge transfer, and reduces the bimolecular recombination. The researchers found that the PCE of the OSCs based on PM6:Y6 increased from 14.64% to 16.25% by adding the optimum concentration of 0.05 wt% $Ti_3C_2T_x$ into the active layer, as exhibited in **Figure 4**g,h.

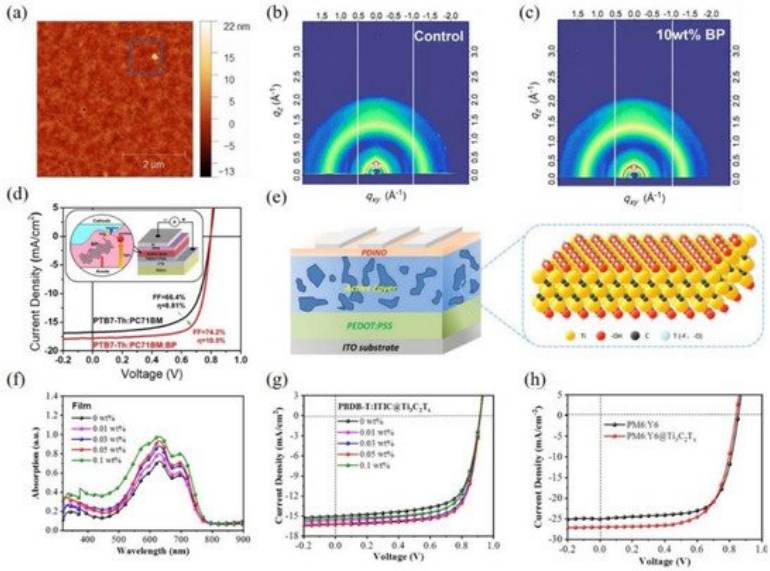

Figure 4. (**a**) AFM height images for PTB7-Th:$PC_{71}BM$:BP blend film; 2D GIWAXS patterns of PTB7-Th:$PC_{71}BM$:BP blend films with various concentration of BP: (**b**) 0 wt% and (**c**) 10 wt%; (**d**) J-V curves of a reference device and the best OSCs with the addition of BP. Inset: The structure of devices and the schematic diagram of light absorption, exciton migration, and separation; (**e**) The structure of OSCs and the schematic structure of $Ti_3C_2T_x$; (**f**) UV-vis absorption spectra of PBDB-T:ITIC doped with different concentration of $Ti_3C_2T_x$, and (**g**) the related J-V curves of the corresponding OSCs; (**h**) The optimal J-V curves of PM6:Y6@$Ti_3C_2T_x$ (0.05 wt%)-based devices. Reprinted with permission form [67][79]. Copyright 2018 Elsevier Ltd. and 2021 John Wiley and Sons.

The main working mechanisms of the 2D materials as additives in the active layer of the OSCs we mentioned above can be concluded as follows: (1) Expand the light absorption range of the active layer; (2) modify the energy levels of heterojunctions for effectively improved the charge transfer; (3) act as conductive bridges or optimize the domain sizes in the heterojunction to increase charge transport. We partly summarized the applications of 2D materials as additives in the active layer for the enhancement of the device efficiency beyond 7% in **Table 2**. The breakthroughs of the efficiency and stability of the OSCs could be expected by adding suitable 2D materials into active layer, as the solubility of more 2D materials can be improved.

Table 2. 2D layer materials incorporated into the active layer of the OSC with PCE over 7%.

NO.	Materials	Function	Device Structure	Jsc (mA/cm^2)	Voc (V)	FF (%)	PCE (%)	PCE Enhancement (%)	Year	R
1	TPP:GO	AL	ITO/PEDOT:PSS/PTB7:$PC_{71}BM$:TPP:GO/MoO_3/Au	18.27	0.78	63	8.81	19.21	2015	[6
2	WSe_2	AL	Glass/ITO/PFN/PTB7:WSe_2:PCBM/MoO_3/Al	17.84	0.73	72	9.45	16.67	2017	[6
3	$MoSe_2$	AL	ITO/ZnO/PBDTTBO:IT-4F:$MoSe_2$/MoO_3/Ag	19.37	0.73	56	7.92	8.13	2019	[6
4	$MoSe_2$	AL	ITO/ZnO/PTB7-TH:$PC_{71}BM$:$MoSe_2$/MoO_3/Ag	18.69	0.78	70	10.44	15.74	2019	[6
5	BP	AL	ITO/PEDOT:PSS/PTB7-Th:$PC_{71}BM$:BP/PFN/Al	18.00	0.80	75	10.50	19.18	2018	[6
6	BP	AL	ITO/ZnO/J71:ITIC:BP/MoO_3/Al	16.6	0.95	60	9.41	11.89	2018	[6
7	BP	AL	ITO/ZnO/PTB7-Th:IEICO-4F:BP/MoO_3/Ag	23.44	0.71	70	12.2	12.96	2019	[6
8	Bi_2O_2S	AL	ITO/ZnO/PTB7:$PC_{71}BM$:Bi_2O_2S/MoO_3/Ag	19.25	0.79	70	10.71	21.84	2019	[7
9	Bi_2O_2Se	AL	ITO/ZnO/PBDB-T:ITIC:Bi_2O_2Se/MoO_3/Ag	17.88	0.93	73	12.22	21.22	2020	[7
10	Bi_2O_2Se	AL	ITO/ZnO/PM6:Y6:Bi_2O_2Se/MoO_3/Ag	25.18	0.84	77	16.28	11.58	2020	[7
11	$Ti_3C_2T_x$	AL	ITO/PEDOT:PSS/PM6:Y6:$Ti_3C_2T_x$/PDINO/Al	27.02	0.840	72	16.25	10.99	2021	[7
12	$Ti_3C_2T_x$	AL	ITO/PEDOT:PSS/PBDB-T:IT-M:$Ti_3C_2T_x$/PDINO/Al	17.65	0.94	60	9.96	10.05	2021	[7
13	$Ti_3C_2T_x$	AL	ITO/PEDOT:PSS/PBDB-T:ITIC:$Ti_3C_2T_x$/PDINO/Al	16.28	0.92	72	10.72	14.8	2021	[7

References

1. Stylianakis, M.M.; Konios, D.; Kakavelakis, G. Efficient ternary organic photovoltaics incorporating a graphene-based porphyrin molecule as a universal electron cascade material. Nanoscale 2015, 7, 17827–17835.
2. Kakavelakis, G.; Castillo, A.E.D.; Pellegrini, V. Size-Tuning of WSe2 Flakes for High Efficiency Inverted Organic Solar Cells. ACS Nano 2017, 11, 3517–3531.
3. Wang, H.C.; Lin, Y.C.; Chen, C.H. Hydrogen plasma-treated MoSe2 nanosheets enhance the efficiency and stability of organic photovoltaics. Nanoscale 2019, 11, 17460–17470.
4. Zhao, Y.; Chen, T.L.; Xiao, L.G. Facile integration of low-cost black phosphorus in solution-processed organic solar cells with improved fill factor and device efficiency. Nano Energy 2018, 53, 345–353.
5. Yang, W.T.; Ye, L.; Yao, F.F. Black phosphorus nanoflakes as morphology modifier for efficient fullerene-free organic solar cells with high fill-factor and better morphological stability. Nano Res. 2019, 12, 777–783.
6. Huang, C.W.; Yu, H.Z.; Chen, J.Y. Improved performance of polymer solar cells by doping with Bi2O2S nanocrystals. Sol. Energy Mater. Sol. Cells 2019, 200, 110030.
7. Huang, C.W.; Yu, H.Z. Two-Dimensional Bi2O2Se with High Mobility for High-Performance Polymer Solar Cells. ACS Appl. Mater. Interfaces 2020, 12, 19643–19654.
8. Zhao, Y.; Liu, X.J.; Jing, X. Addition of 2D Ti3C2TX to Enhance Photocurrent in Diodes for High-Efficiency Organic Solar Cells. Solar RRL 2021, 5, 2100127.
9. Gu, X.; Cui, W.; Li, H. A Solution-Processed Hole Extraction Layer Made from Ultrathin MoS2 Nanosheets for Efficient Organic Solar Cells. Adv. Energy Mater. 2013, 3, 1262–1268.
10. Gu, X.; Cui, W.; Song, T. Solution-Processed 2D Niobium Diselenide Nanosheets as Efficient Hole-Transport Layers in Organic Solar Cells. Chemsuschem 2014, 7, 416–420.
11. Koo, D.; Jung, S.; Oh, N.K. Improved charge transport via WSe2-mediated hole transporting layer toward efficient organic solar cells. Semicond. Sci. Technol. 2018, 33, 125020.
12. Lin, Y.B.; Adilbekova, B.; Firdaus, Y. 17% Efficient Organic Solar Cells Based on Liquid Exfoliated WS2 as a Replacement for PEDOT:PSS. Adv. Mater. 2019, 31, 1902965.
13. Yusoff, A.R.B.; Kim, D.; Schneider, F.K. Au-doped single layer graphene nanoribbons for a record-high efficiency ITO-free tandem polymer solar cell. Energy Environ. Sci. 2015, 8, 1523–1537.
14. Yu, J.C.; Jang, J.I.; Lee, B.R. Highly Efficient Polymer-Based Optoelectronic Devices Using PEDOT:PSS and a GO Composite Layer as a Hole Transport Layer. ACS Appl. Mater. Interfaces 2014, 6, 2067–2073.
15. Cheng, X.F.; Long, J.; Wu, R. Fluorinated Reduced Graphene Oxide as an Efficient Hole-Transport Layer for Efficient and Stable Polymer Solar Cells. ACS Omega 2017, 2, 2010–2016.
16. Cheng, J.Q.; Zhang, H.; Zhao, Y. Self-Assembled Quasi-3D Nanocomposite: A Novel p-Type Hole Transport Layer for High Performance Inverted Organic Solar Cells. Adv. Funct. Mater. 2018, 28, 1706403.
17. Huang, C.W.; Yu, H.Z.; Chen, J.Y. Improved performance of polymer solar cells by doping with Bi2O2S nanocrystals. Sol. Energy Mater. Sol. Cells 2019, 200, 110030.
18. Wu, J.X.; Yuan, H.T.; Meng, M.M. High electron mobility and quantum oscillations in non-encapsulated ultrathin semiconducting Bi2O2Se. Nat. Nanotechnol. 2017, 12, 530–534.
19. Li, M.Q.; Dang, L.Y.; Wang, G.G. Bismuth Oxychalcogenide Nanosheet: Facile Synthesis, Characterization, and Photodetector Application. Adv. Mater. Technol. 2020, 5, 2000180.
20. Fatima, M.J.J.; Navaneeth, A.; Sindhu, S. Improved carrier mobility and bandgap tuning of zinc doped bismuth oxide. RSC Adv. 2015, 5, 2504–2510.
21. Leontie, L.; Caraman, M.; Alexe, M. Structural and optical characteristics of bismuth oxide thin films. Surf. Sci. 2002, 507, 480–485.
22. Wu, J.X.; Qiu, C.G.; Fu, H.X. Low Residual Carrier Concentration and High Mobility in 2D Semiconducting Bi2O2Se. Nano Lett. 2019, 19, 197–202.
23. Huang, C.W.; Yu, H.Z. Two-Dimensional Bi2O2Se with High Mobility for High-Performance Polymer Solar Cells. ACS Appl. Mater. Interfaces 2020, 12, 19643–19654.
24. Naguib, M.; Kurtoglu, M.; Presser, V. Two-Dimensional Nanocrystals Produced by Exfoliation of Ti3AlC2. Adv. Mater. 2011, 23, 4248–4253.
25. Lei, J.C.; Zhang, X.; Zhou, Z. Recent advances in MXene: Preparation, properties, and applications. Front. Phys. 2015, 10, 276–286.

26. Zhao, Y.; Liu, X.J.; Jing, X. Addition of 2D Ti3C2TX to Enhance Photocurrent in Diodes for High-Efficiency Organic Solar Cells. Solar RRL 2021, 5, 2100127.
27. Yang, Q.; Yu, S.W.; Fu, P. Boosting Performance of Non-Fullerene Organic Solar Cells by 2D g-C3N4 Doped PEDOT:PSS. Adv. Funct. Mater. 2020, 30, 1910205.
28. Fernandez-Arteaga, Y.; Maldonado, J.L.; Nicasio-Collazo, J. Solution processable graphene derivative used in a bilayer anode with conductive PEDOT:PSS on the non-fullerene PBDB-T:ITIC based organic solar cells. Sol. Energy 2021, 225, 656–665.
29. Wang, J.; Peng, R.X.; Gao, J. Ti3C2TX/PEDOT:PSS Composite Interface Enables over 17% Efficiency Non-fullerene Organic Solar Cells. ACS Appl. Mater. Interfaces 2021, 13, 45789–45797.
30. Bao, Z.Y.; Liu, S.H.; Hou, Y.D. Hollow Au nanorattles for boosting the performance of organic photovoltaics. J. Mater. Chem. A 2019, 7, 26797–26803.
31. Hou, C.L.; Yu, H.Z. Modifying the nanostructures of PEDOT:PSS/Ti3C2TX composite hole transport layers for highly efficient polymer solar cells. J. Mater. Chem. C 2020, 8, 4169–4180.
32. Socol, M.; Preda, N. Hybrid Nanocomposite Thin Films for Photovoltaic Applications: A Review. Nanomaterials 2021, 11, 1117.
33. Eisner, F.; Seitkhan, A.; Han, Y. Solution-Processed In2O3/ZnO Heterojunction Electron Transport Layers for Efficient Organic Bulk Heterojunction and Inorganic Colloidal Quantum-Dot Solar Cells. Solar RRL 2018, 2, 1800076.
34. In, S.J.; Park, M.; Jung, J.W. Reduced interface energy loss in non-fullerene organic solar cells using room temperature-synthesized SnO2 quantum dots. J. Mater. Sci. Technol. 2020, 52, 12–19.
35. Liu, S.H.; Hou, Y.D.; Xie, W. Quantitative Determination of Contribution by Enhanced Local Electric Field, Antenna-Amplified Light Scattering, and Surface Energy Transfer to the Performance of Plasmonic Organic Solar Cells. Small 2018, 14, 1800870.
36. Yuan, J.B.; Zhang, X.L.; Sun, J.G. Hybrid Perovskite Quantum Dot/Non-Fullerene Molecule Solar Cells with Efficiency Over 15%. Adv. Funct. Mater. 2021, 31, 2101272.
37. Ahmed, E.; Ren, G.Q.; Kim, F.S. Design of New Electron Acceptor Materials for Organic Photovoltaics: Synthesis, Electron Transport, Photophysics, and Photovoltaic Properties of Oligothiophene-Functionalized Naphthalene Diimides. Chem. Mater. 2011, 23, 4563–4577.
38. Liu, S.H.; Zhang, Y.Y.; Lin, Y. Tailoring the structure and nitrogen content of nitrogen-doped carbon nanotubes by water-assisted growth. Carbon 2014, 69, 247–254.
39. Ren, G.Q.; Ahmed, E.; Jenekhe, S.A. Nanowires of oligothiophene-functionalized naphthalene diimides: Self assembly, morphology, and all-nanowire bulk heterojunction solar cells. J. Mater. Chem. 2012, 22, 24373–24379.
40. Wang, Y.F.; Jia, B.Y.; Qin, F. Semitransparent, non-fullerene and flexible all-plastic solar cells. Polymer 2016, 107, 108–112.
41. Zhao, F.G.; Deng, L.L.; Wang, K. Surface Modification of SnO2 via MAPbI3 Nanowires for a Highly Efficient Non-Fullerene Acceptor-Based Organic Solar Cell. ACS Appl. Mater. Interfaces 2020, 12, 5120–5127.
42. Butun, S.; Tongay, S.; Aydin, K. Enhanced Light Emission from Large-Area Monolayer MoS2 Using Plasmonic Nanodisc Arrays. Nano Lett. 2015, 15, 2700–2704.
43. Chen, Y.N.; Sun, Y.; Peng, J.J. Tailoring Organic Cation of 2D Air-Stable Organometal Halide Perovskites for Highly Efficient Planar Solar Cells. Adv. Energy Mater. 2017, 7, 1700162.
44. Fan, Q.P.; Zhu, Q.L.; Xu, Z. Chlorine substituted 2D-conjugated polymer for high-performance polymer solar cells with 13.1% efficiency via toluene processing. Nano Energy 2018, 48, 413–420.
45. Ling, H.F.; Liu, S.H.; Zheng, Z.J. Organic Flexible Electronics. Small Methods 2018, 2, 1800070.
46. Ma, C.Q.; Shen, D.; Ng, T.W. 2D Perovskites with Short Interlayer Distance for High-Performance Solar Cell Application. Adv. Mater. 2018, 30, 1800710.
47. Das, S.; Pandey, D.; Thomas, J. The Role of Graphene and Other 2D Materials in Solar Photovoltaics. Adv. Mater. 2019, 31, 1802722.
48. Liu, Z.K.; Lau, S.P.; Yan, F. Functionalized graphene and other two-dimensional materials for photovoltaic devices: Device design and processing. Chem. Soc. Rev. 2015, 44, 5638–5679.
49. Zhou, H.L.; Wang, C.; Shaw, J.C. Large Area Growth and Electrical Properties of p-Type WSe2 Atomic Layers. Nano Lett. 2015, 15, 709–713.
50. Zhang, Y.; Chang, T.-R.; Zhou, B. Direct observation of the transition from indirect to direct bandgap in atomically thin epitaxial MoSe2. Nat. Nanotechnol. 2014, 9, 111–115.

51. Wu, M.; Zeng, X.C. Bismuth Oxychalcogenides: A New Class of Ferroelectric/Ferroelastic Materials with Ultra High Mobility. Nano Lett. 2017, 17, 6309–6314.
52. Meng, S.; Wang, J.; Shi, H. Distinct ultrafast carrier dynamics of α-In2Se3 and β-In2Se3: Contributions from band filling and bandgap renormalization. Phys. Chem. Chem. Phys. 2021, 23, 24313–24318.
53. Akinwande, D.; Petrone, N.; Hone, J. Two-dimensional flexible nanoelectronics. Nat. Commun. 2014, 5, 5678.
54. Nguyen, V.H.; Nguyen, B.S.; Hu, C.C. Novel Architecture Titanium Carbide (Ti3C2TX) MXene Cocatalysts toward Photocatalytic Hydrogen Production: A Mini-Review. Nanomaterials 2020, 10, 602.
55. Garg, R.; Dutta, N.K.; Choudhury, N.R. Work Function Engineering of Graphene. Nanomaterials 2014, 4, 267–300.
56. Suh, J.; Park, T.E.; Lin, D.Y. Doping against the Native Propensity of MoS2: Degenerate Hole Doping by Cation Substitution. Nano Lett. 2014, 14, 6976–6982.